

IIT MMAE 414  
Crop Duster  
Conceptual Design Report

**Group 8**

Mason Rinkel

Evelina Cojocaru Visinschi

Peter Mayer

Jonah Wilkes

Ty Garrison

## Contents

1. Executive summary

2. System requirements review

    2.1 Introduction and Motivation

    2.2 Historical Summary of Agricultural Aircraft Market

    2.3 Design Requirements

    2.4 Design Mission Profile

    2.5 Ferry Mission Profile

    2.6 Design Approach

    2.7 Initial Sizing

        2.7.1 Specific Fuel Consumption (SFC) Initial Estimation

        2.7.2 Wing Loading (W/S) Selection

        2.7.3 Trade Study Analysis

        2.7.4 Fuel Fraction Estimation

        2.7.5 Empty Weight Fraction

        2.7.6 Gross Weight Estimation

3. Aerodynamics

    3.1 Airfoil Selection

    3.2 Selection Matrix

    3.3 Wing Sizing

4. Propulsion

    4.1 Engine Selection

    4.2 Propeller Diameter

## 5. Structures

5.1 FEA

5.2 V-n Diagram

5.3 Dihedral

5.4 Sizing

## 6. Cost analysis

6.1 Weight Based Analysis

6.2 DAPCA-IV Model

## 7. Conclusion

## References

## List of figures

2.1 Design Mission Profile

2.2 Ferry Mission Profile

2.3  $W_0$  and TOP limit curves on the P/W vs W/S design space.

3.1 Lift coefficient versus angle of attack for the NACA 2412, 4412, and 4415 airfoils

3.2 Lift-to-drag ratio and drag polar for the NACA airfoils

3.3 Drag and pitching-moment coefficients versus angle of attack for the NACA airfoils

4.1 PT6A Engine

4.2 TPE331 Engine

5.1 - Elliptical lift distribution on wing

5.2 - Wing flexure in inches under MTOW load

5.3 - Stress analysis on half-wing with MTOW load

5.4 - Factor of safety analysis under MTOW load

5.5 - V-n Diagram for crop duster

5.6 - Aircraft sizing sketch

6.1 - RDT&E and Production Cost Breakdown

6.2 - Breakeven Analysis

## 1. Executive Summary

A crop duster that meets the performance, capability, and safety requirements was designed. In this conceptual design report are presented details of all the designing processes. Those include such major sections as aerodynamics, propulsion, structures, and cost analysis.

As part of the aerodynamics design airfoil selection using the matrix method, wing sizing and geometry are considered. For the propulsion the best engine for the design mission selection was made using the selection matrix method, and the propeller diameter calculation are described. For structures, the finite element analysis, V-n diagram, dehidral, sizing are discussed. The cost analysis included the consideration of the gross and empty weight of the aircraft, in accordance to Raymer and in comparison to the existing Air Tractor AT-802. Another approach used in the cost analysis was the DAPCA-IV method that proves to be more accurate.

### Organization chart

Section	Lead	Secondary
Leader	Evelina Cojocaru Visinschi	Peter Mayer
Aerodynamics	Jonah Wilkes	Ty Garrison
Cost Analysis	Ty Garrison	Mason Rinkel
Propulsion	Mason Rinkel	Evelina Cojocaru Visinschi
Structures	Peter Mayer	Jonah Wilkes

**Table 1.1**

## 2. System requirements review

### 2.1. Introduction and Motivation

The conversion and design of fixed-wing agricultural aircraft is geared towards aerial application of various agricultural products including pesticides, fertilizers and seed. The main aim is to enhance crop production, minimize labor costs, and rapidly respond to crop pests and diseases. The applied motivations for aerial applications can be economic (intensive farming), technical (immediate response to crop threats), and sociopolitical (government production control measures).

While aviation in agriculture has operated efficiently for nearly a century, safety issues in agricultural aviation remain. 3,102 accidents occurred during a 28-year period, and approximately 10% were fatal according to a retrospective study by Van Doon on aircraft under 14 CFR 137. 27% of crashes resulting in fatalities due to collision with obstacles during low-altitude maneuvering and landing are attributed to human error. Recommended measures to reduce these accidents include obstacle marking and low-altitude navigation. Moreover, unmanned Aircraft Systems (UAS) safety issues are a response to the potential of mid-air collisions with general aviation aircraft.

The motivation behind this project is to introduce an unmanned aircraft design that will suffice the FAA requirements, assist in making the agricultural aircraft use more sustainable and safer, as well as, have an improved efficiency in the food-supply agricultural process.

### 2.2. Historical Summary of Agricultural Aircraft Market

In 1919, the United States Department of Agriculture first utilized aircraft for pest-control cotton field reconnaissance. The first crop dusting experiment took place in 1921, when Lt. John A. Macready used a modified Curtiss JN-4 to dust catalpa trees with lead arsenate to kill sphinx moth larvae. Agricultural aviation began with dusting and reconnaissance and expanded to become a fully integrated aviation sector. The first surplus-constructed WWI Curtiss JN-6H and Airco DH-4 and crop-dusting aircraft were conceived. These aircraft were unstable and unsafe at low altitudes, nonetheless, they were the precursors of present-day ag aircraft.

#### Overview of the Present Market

According to DATAIntelo, the global agricultural aircraft market was valued at USD 5.5 billion in 2023 and is anticipated to reach USD 9.8 billion by 2032, with a growth of USD 5.5 billion by 2032, with a growth of USD 5.5 billion by 2032, with a growth of CAG of 6.8%. Growth is spurred by precision agriculture, technological advancements, and increased demand for efficient crop management.

### Market Growth Contributors

- Precision agriculture—The ability to monitor crops and automatically irrigate them fuels the need for aerial data collection.
- Technological advancements—The advent of UAVs, advanced propulsion systems, and avionics changes the landscape of aerial operations.
- Growing crop protection—The increasing demand for food drives aerial spraying of pesticides and fertilizers.
- Expansion of the agrochemical industry—Increased demand for aircraft for aerial distribution of chemicals.
- Sustainability—Targeted spraying and environmentally sustainable practices improve the market's appeal.
- Rest Market Restraints:
- High initial Investment: Significant capital is needed to acquire these systems, creating market entry challenges for small farmers.
- Limited awareness Adoption of these advancements.: Conventional ensuing farmers are unaware of these new advancements.
- Environmental concerns: Spraying systems should be properly regulated due to potential overspray, and ensuing chemicals.
- Limited awareness of these advancements. Converting farmers to these practices.

### Segmentation by Application

- Crop dusting, pest management, fertilizing, and seeding are completed in a quick and uniform manner over extensive or hard-to-reach regions.

### Segmentation by End User

- Farmers (direct users seeing improved yields),
- Agricultural service providers (crop-spraying service)
- Government agencies (research, disaster assessment, and regulation).

### Geographical Breakdown

- North America: Technology leader in large-scale agriculture.
- Europe: Sustainable and eco-friendly farming practices.
- Asia-Pacific: Rising food demand and modernization makes this the fastest-growing.
- Middle East & Africa: Slow but developing adoption through agricultural development.
- Latin America: Diverse agriculture providing emerging opportunities.

Thrush Aircraft, Air Tractor, Cessna, Embraer, Boeing, Grob Aircraft, Grumman Ag Cat, Gippsland GA200, Dynali, and PZL-106 Kruk are a few major players.

## 2.3. Design Requirements

**Table 2.1 Design Mission Requirements**

Category	Requirement	Specification
<b>Performance</b>	Operational radius	50 nmi
	Design radius	25 nmi
	Fuel reserve	$\geq 15$ minutes after mission completion
	Maximum gross weight	< 19,000 lb
	Maximum flight speed	< 250 kts
	Takeoff ground run	$\leq 1,000$ ft
	Takeoff distance over 50 ft obstacle	$\leq 1,500$ ft
	Runway surface	Hard-packed dirt or grass
<b>Mission Capability</b>	Agricultural dusting	Must dust 400 acres of land
	Operating environment	ISA, 1,791 ft elevation, 30°F
<b>Certification &amp; Safety</b>	Regulatory compliance	FAA 14 CFR Part 137
	Remote control latency (if unmanned)	< 100 ms
	Reliability (unmanned)	Probability of Hull Loss $\leq 1 \times 10^{-9}$ flight hours
	Reliability (manned)	Probability of Fatal Event $\leq 1 \times 10^{-6}$ flight hours

**Table 2.2 Ferry Mission Requirements**

Category	Requirement	Specification
<b>Performance</b>	Cruise range	600 nmi
	Fuel reserve	$\geq 15$ minutes after mission completion
	Maximum gross weight	$< 19,000$ lb
	Maximum flight speed	$< 250$ kts
	Flight altitude	ISA, 1,000 ft elevation, 30°F
	Takeoff ground run	$\leq 1,000$ ft
	Takeoff distance over 50 ft obstacle	$\leq 1,500$ ft
	Runway surface	Hard-packed dirt or grass
<b>Payload &amp; Safety</b>	Payload	Minimum of one pilot, full visibility, and safety compliance
	Flight control system	Fully reversible or fly-by-wire
	Reliability	Probability of Fatal Event $\leq 1 \times 10^{-9}$ flight hours
	Certification	FAA 14 CFR Part 137

## 2.4. Design Mission Profile

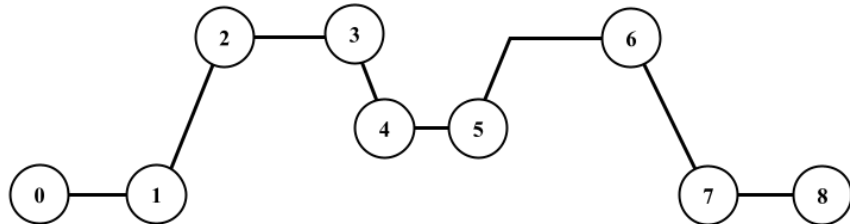


Figure 2.1: Design Mission Profile

The first profile that will be used by the crop duster is the low-level mission profile. The low-level strike profile is meant to efficiently cover large agricultural areas for applying chemicals, seeds, or fertilizers, minimizing soil compaction and ensuring timely delivery of treatments through the weight-drop phase.

Following are the phases by which this profile is built on:

0-1: Warmup and Takeoff

1-2: Climb

2-3: Cruise out

3-4: Loiter

4-5: Weight Drop

5-6: Cruise back

6-7: Loiter

7-8: Land

## 2.5. Ferry Mission Profile

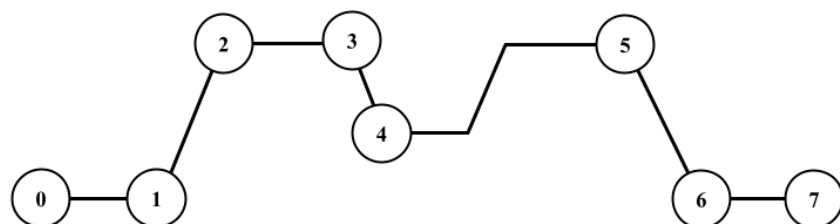


Figure 2.2: Ferry Mission Profile

During the Ferry Mission the crop duster will be flown by a pilot from one location to another, generally from field to field, or to the agricultural hangar. This profile lacks the Weight Drop phase from the Design Mission profile.

Following are the phases by which this profile is built on:

0-1: Warmup and Takeoff

1-2: Climb

2-3: Cruise out

3-4: Loiter

4-5: Climb and Cruise back

5-6: Loiter

6-7: Land

## 2.6. Design Approach

The design approach follows a structured, requirements-driven process informed by mission objectives and empirical methods from *Aircraft Design: A Conceptual Approach* (Raymer, 2018). Initial parameters for wing loading, power-to-weight ratio, and fuel fraction were derived from comparable agricultural aircraft and refined through iterative analyses of aerodynamics, propulsion, and structures. Each subsystem was developed concurrently to ensure coherence between aerodynamic, structural, and propulsion objectives. The methodology prioritized efficient low-speed handling and dependable short-field performance while maintaining balanced weight distribution and stability. Iterative refinement of these elements produced a cohesive configuration capable of meeting the operational demands of agricultural flight.

## 2.7. Initial Sizing

Initial sizing establishes the preliminary weight and performance characteristics of the aircraft based on mission requirements and general configuration assumptions. This step provides first-order estimates of specific fuel consumption, fuel fraction, empty weight, gross weight, and wing loading, which collectively define the overall scale and feasibility of the design. These parameters are derived using empirical relationships and regression data from *Aircraft Design: A Conceptual Approach* (Raymer, 2018) and are later refined through detailed aerodynamic, structural, and propulsion analyses in subsequent sections.

### 2.7.1 Specific Fuel Consumption (SFC) Initial Estimation

The specific fuel consumption (SFC) establishes the fuel efficiency of the propulsion system and is a key driver in the weight and range calculations. According to *Aircraft Design: A Conceptual Approach* (Raymer, 2018, Table 3.4), typical turboprop engines exhibit cruise SFC values in the range of  $0.45 - 0.55 \text{ hr}^{-1}$  and loiter SFC values near  $0.6 \text{ hr}^{-1}$ . Because the current design utilizes a turboprop configuration similar to modern agricultural aircraft such as the Thrush 710P and Air Tractor 802A, the corresponding expected values were taken as  $0.5 \text{ hr}^{-1}$  for cruise and  $0.6 \text{ hr}^{-1}$  for loiter conditions.

### 2.7.2 Wing Loading (W/S) Selection

The wing loading, W/S, determines the balance between aerodynamic efficiency and low-speed performance. Agricultural aircraft require low wing loadings to ensure short takeoff distance, low stall speed, and stable handling during spray operations. Existing crop dusters span a wide range of values: the Cessna 188 AgWagon operates near  $18 \text{ lb/ft}^2$ , favoring maneuverability but sacrificing cruise efficiency, while the Air Tractor AT-802A approaches  $40 \text{ lb/ft}^2$ , offering higher payload capability at the cost of longer takeoff runs. These values are displayed in Table 3.1

Because the current design is constrained primarily by takeoff distance—operating from short, unpaved agricultural strips—a baseline wing loading of  $25 \text{ lb/ft}^2$  is selected. This value provides a practical compromise between the low-speed agility of lighter aircraft and the

efficiency of larger turboprop designs. It will serve as the initial sizing parameter and may be refined following detailed performance analyses in later sections (Raymer, 2018).

### 2.7.3 Trade Study Analysis

To further validate the chosen design parameters, a trade study was performed varying both the power-to-weight ratio ( $P/W$ ) and wing loading ( $W/S$ ) to evaluate their combined influence on takeoff performance and overall feasibility. The results are illustrated in Figure 2.X, which plots contours of constant gross weight alongside takeoff parameter (TOP) constraints. The red boundary represents the  $\text{TOP} = 170$  limit, with the shaded region below indicating configurations that exceed acceptable takeoff distance. Based on this analysis, the selected design point— $T/W = 0.1308$  and  $W/S = 25 \text{ lb}/\text{ft}^2$ —lies within the feasible region, corresponding to a takeoff parameter of approximately  $\text{TOP} = 158$ . This point provides an optimal balance between field performance and power efficiency and is therefore adopted for all subsequent design estimates.

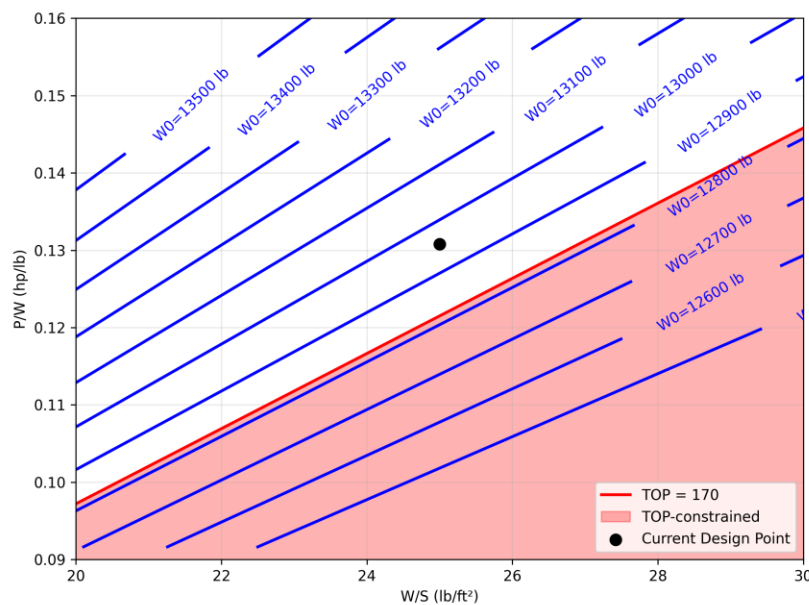


**Figure 2.3**  $W_0$  and TOP limit curves on the  $P/W$  vs  $W/S$  design space.

### 2.7.4 Fuel Fraction Estimation

Two mission profiles were developed to satisfy the design criteria: a design mission and a ferry mission. For both profiles, an aerodynamic efficiency of  $(L/D)_{\max} = 13.3$  was assumed as calculated in section 3, based on the value derived in the preceding section. The specific fuel consumption (SFC) was defined as  $0.5 \text{ hr}^{-1}$  during cruise and  $0.6 \text{ hr}^{-1}$  during loiter, with a constant cruise velocity of  $280 \text{ ft/s}$  (166 kt).

The design mission includes the following flight phases: takeoff, climb, cruise to the target field (maximum range of 50 nmi, equivalent to 304,000 ft), a 30-minute loiter period to prepare for spraying operations, payload release, return cruise to base, final loiter and approach, and landing. A payload drop weight ratio of unity was assumed. Fuel fractions for the cruise and

## Conceptual Design Report

Loiter phases were computed using Equations 3.6 and 3.8 from *Aircraft Design: A Conceptual Approach* (Raymer, 2018), and the total fuel fraction was obtained using Equation 3.13. The resulting weight ratios for the design mission are summarized in Table 2.3.

**Table 2.3** Weight Ratios from the Design mission profile.

Phase	Ratio	Value
Takeoff	W1/W0	0.97
Climb	W2/W1	0.985
Cruise	W3/W2	0.9887
Loiter	W4/W3	0.9743
Payload Drop	W5/W4	1
Cruise	W6/W5	0.9887
Loiter	W7/W8	0.9743
Land	W8/W7	0.995
Result	W8/W0	0.8822
Fuel Ratio	Wf/W0	0.1249

The ferry mission was defined to simulate long-range repositioning without payload. This mission includes takeoff, climb, cruise to a new location, loiter and landing preparation, a diversion leg, additional loiter for final approach, and landing. A nominal payload of 300 lb was assigned to account for the pilot and small onboard items. The loiter duration was extended to one hour, and the cruise range increased to 600 nmi (3,645,000 ft). The same L/D<sub>max</sub>, SFC, and cruise velocity values used in the design mission were retained. The corresponding weight ratios for the ferry mission are presented in Table 2.4.

**Table 2.4** Weight Ratios from the Ferry mission profile.

Phase	Ratio	Value
Takeoff	W1/W0	0.97
Climb	W2/W1	0.985
Cruise	W3/W2	0.8729
Loiter	W4/W3	0.9492
Cruise	W5/W4	0.8729
Loiter	W6/W5	0.9492
Land	W7/W6	0.995
Result	W7/W0	0.6527
Fuel Ratio	Wf/W0	0.3682

The total fuel fractions for the design and ferry missions are therefore 0.1249 and 0.3682, respectively. These values are consistent with typical estimates for propeller-driven agricultural aircraft (Raymer, 2018).

## **2.7.5 Empty Weight Fraction**

The empty weight fraction was estimated using the empirical coefficients for agricultural aircraft provided in *Aircraft Design: A Conceptual Approach* (Raymer, 2018, Table 3.1). The coefficients  $A=0.74$  and  $C= -0.03$  were applied to Raymer's empirical weight fraction relation (Equation 3.1), assuming a variable-sweep correction factor of 1.0. This approach was implemented iteratively alongside the gross weight estimation described in the following section.

The resulting empty weight fractions were 0.5539 for the design mission and 0.5729 for the ferry mission. These values are slightly higher than those reported in Raymer's (2018) examples, which may be attributed to the lower payload fraction and specialized structural requirements of agricultural aircraft, including reinforced wings and payload compartments for chemical dispersal systems.

## **2.7.6 Gross Weight Estimation**

An initial gross weight estimate of 19,000 lb was assumed and refined iteratively using Equation 3.4 from *Aircraft Design: A Conceptual Approach* (Raymer, 2018). For the design mission, a payload of 4,000 lb was assigned, resulting in a converged gross weight of 12,600 lb. For the ferry mission, which included only crew and minimal cargo (300 lb), the gross weight converged to 5,100 lb.

The design mission estimate aligns closely with published data for comparable aircraft such as the Thrush 710P and Air Tractor AT-802, as presented in Table 3.1, while the ferry mission estimate corresponds with smaller agricultural configurations. The slightly lower gross weight predicted for the current design likely results from a conservative payload reduction to ensure compliance with power-to-weight requirements for short-runway operations.

### 3 Aerodynamics

Agricultural aircraft occupy a distinct niche in aviation design. Unlike transport or passenger aircraft optimized for range or efficiency, agricultural aircraft are designed to perform low-altitude, high-precision, and high-frequency missions over confined agricultural areas. This mission environment imposes severe design constraints: flight paths as low as a few feet above ground level, repeated pull-ups and turns under high load factors, and large variations in weight as payload is expended are among the most important factors for consideration. The aircraft must therefore achieve exceptional lift performance, structural robustness, and controllability at low speeds.

#### 3.1 Airfoil Selection

To meet these constraints, several baseline assumptions must be made about the design. To sustain lift at low operating speeds, the aircraft will require a relatively large wing with a moderate aspect ratio, in contrast to the high-speed, high wing-loading designs of jet aircraft. Given the substantial payloads carried during spraying operations, the wing and airfoil must generate high lift coefficients while maintaining stable handling characteristics, even under varying load conditions. This necessitates the use of a high-lift, thicker airfoil capable of achieving elevated  $C_L$  values and delaying the impact of stall conditions.

To establish a baseline for sizing and airfoil selection, several existing agricultural aircraft were analyzed, including the Cessna 188 AgWagon, Grumman G-164 Ag-Cat, Thrush 710P, and Air Tractor AT-802. These aircraft provide representative examples across a range of payload capacities, powerplants, and design eras, offering valuable reference points for both geometric and aerodynamic characteristics. The corresponding reference values are summarized in Table 3.1. The Cessna 188 and Ag-Cat, for instance, feature moderate wing spans and lower gross weights suited to small-scale operations, typically employing NACA 23000-series or 4412-type airfoils optimized for low-speed lift and docile stall behavior. In contrast, the modern Thrush 710P and Air Tractor 802 represent higher-capacity, turbine-powered designs with significantly greater wing loading and payload capability, while retaining relatively thick, high-lift airfoils to preserve short-field performance. Collectively, these aircraft establish realistic bounds for wing area, aspect ratio, and airfoil thickness that inform the preliminary sizing of the present design.

**Table 3.1** Representative parameters of existing agricultural aircraft used for sizing and airfoil selection reference.

	Cessna 188	Grumman G-164 Ag-Cat	Thrush 710p	Air Tractor AT-802
Gross Weight	3300 lb	4500 lb	14150 lb	16000 lb
Surface Area (S)	205 ft <sup>2</sup>	326 ft <sup>2</sup>	405 ft <sup>2</sup>	401 ft <sup>2</sup>
Wingspan (b)	41.67 ft	35.92 ft	54 ft	59.2 ft
Aspect Ratio	8.47	3.9	7.2	8.74

Wetted Aspect Ratio	2.118	0.97	1.8	2.185
---------------------	-------	------	-----	-------

Three candidate airfoils were selected for the main wing, based on configurations used in existing agricultural aircraft. These include the NACA 2412 employed on the Cessna 188 AgWagon, the NACA 4412 of the Grumman G-164 Ag-Cat, and the NACA 4415 utilized by the Air Tractor AT-802. Agricultural aircraft require relatively thick wing sections to support high structural loads and produce substantial lift at low airspeeds, making the NACA 24- and 44-series airfoils particularly well suited for such applications. The initial aerodynamic analysis for each airfoil was performed in XFLR5 at a Mach number of 0.25 and a Reynolds number of  $1 \times 10^7$ , representative of expected cruise conditions. Although a batch analysis was also conducted to assess performance trends across varying Reynolds numbers, the following results are presented for a single condition to maintain consistency among the compared profiles. These results are summarized in the subsequent tables and plots.

**Table 3.2** Aerodynamic Characteristics of Selected Airfoils at Mach 0.25 and  $Re = 1e7$

	NACA 2412	NACA 4412	NACA 4415
Clmax	1.8887	1.9580	1.9269
CL/CD max	137.40	172.19	174.13
CD_min	0.0052	0.0053	0.0057
Thickness	0.12	0.12	0.15

Figure 3.1 illustrates the lift curve and stall characteristics of the selected airfoils. The NACA 4412 and 4415 exhibit nearly identical maximum lift coefficients ( $C_{L,max} = 1.96$  and 1.93, respectively) at a stall angle of approximately  $17.5^\circ$ , outperforming the NACA 2412, which reaches  $C_{L,max} = 1.89$ . The 2412's lift curve lies consistently below those of the 44-series, indicating less efficient lift generation across the operating range. All three profiles display a linear lift region up to roughly  $15^\circ$ , signifying predictable control and stable handling. The small performance difference between the 4412 and 4415 suggests that either could satisfy the low-speed lift requirements; however, the higher  $C_{L,max}$  of the 44-series directly contributes to shorter takeoff and landing distances, a key advantage for agricultural aircraft operating from unprepared fields.

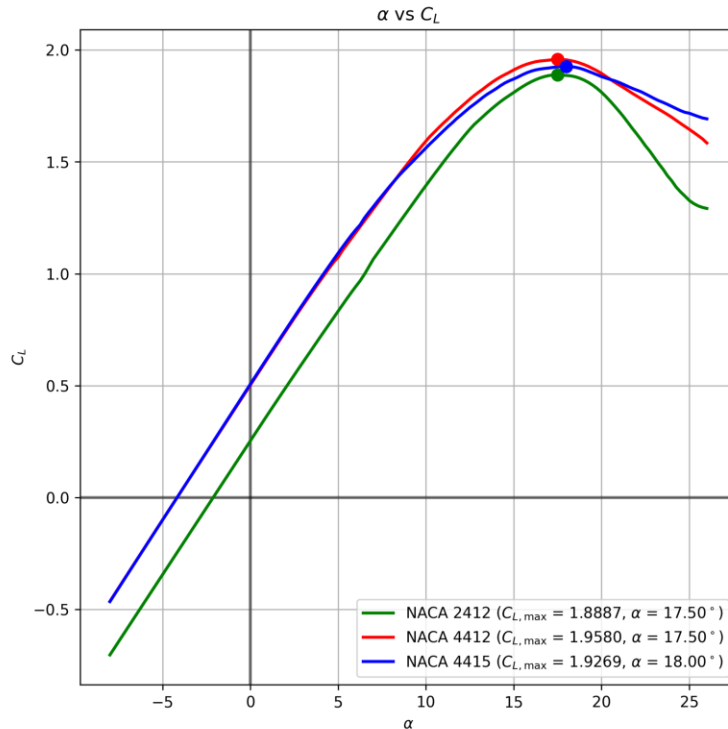


**Figure 3.1** Lift coefficient versus angle of attack for the NACA 2412, 4412, and 4415 airfoils.

Figure 3.2 presents both the aerodynamic efficiency  $C_L/C_D$  variation with angle of attack (left) and the corresponding drag polars ( $C_L$  vs  $C_D$ ) (right) for the three selected airfoils. The NACA 4412 and 4415 achieve markedly higher efficiency peaks of approximately 172 and 174, respectively, at angles of attack near  $5^\circ$ – $6^\circ$ , while the 2412 reaches a lower maximum of about 137 at  $7.25^\circ$ . This indicates that the 44-series profiles deliver superior lift-to-drag performance over a broad operational range, particularly in climb and cruise conditions where moderate lift coefficients dominate.

The drag polars on the right further confirm this trend: the 44-series airfoils produce lower drag for a given lift coefficient, resulting in flatter, more extended efficiency “buckets.” The 2412, by contrast, exhibits a steeper polar curve, implying greater drag penalties at equivalent lift levels. These results demonstrate that the 4412 and 4415 maintain better aerodynamic economy, translating to improved endurance and fuel efficiency during ferry and loiter segments.

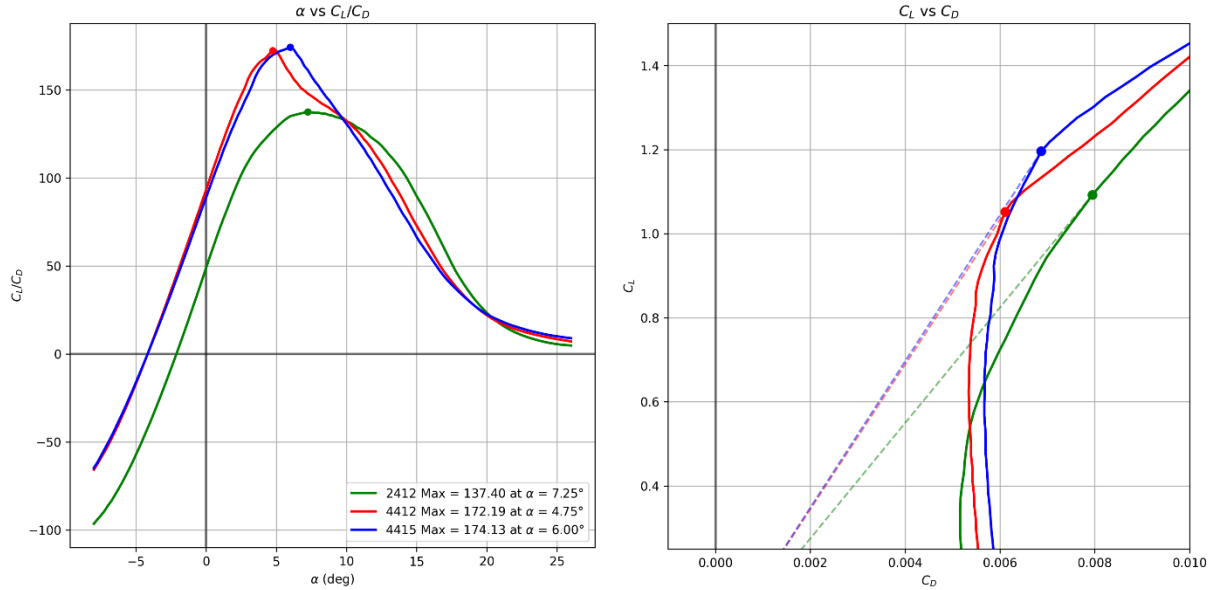


**Figure 3.2** Lift-to-drag ratio and drag polar for the NACA airfoils.

Figure 3.3 compares the drag coefficient and pitching-moment behavior of the three airfoils across the tested angle-of-attack range. The left plot ( $C_D$  vs.  $\alpha$ ) shows that all sections maintain low drag near zero angle of attack, with minimum drag coefficients of approximately 0.0052 for the NACA 2412, 0.0053 for the 4412, and 0.0057 for the thicker 4415. The slight drag increase in the 4415 is a result of its 15 % thickness, which increases frontal area but simultaneously enhances structural depth. Overall, both 44-series airfoils demonstrate comparable drag performance to the thinner 2412 within the linear lift range, with divergence only beyond about 15°, where flow separation drives a rapid drag rise.

The right plot ( $C_m$  vs.  $\alpha$ ) illustrates each airfoil's longitudinal stability tendency. The NACA 2412 exhibits a weaker nose-down pitching moment at zero lift ( $C_{m,0} = -0.0548$ ), while the 4412 and 4415 display stronger negative moments ( $C_{m,0} \approx -0.109$ ). This more negative moment indicates a steeper  $dC_m/d\alpha$  slope and thus a greater static restoring tendency about the pitch axis—desirable for low-altitude, low-speed agricultural operations that demand smooth, self-correcting handling. The 44-series airfoils therefore provide improved inherent stability margins without introducing excessive trim drag. When combined with an appropriately sized horizontal tail, the overall aircraft is expected to exhibit positive static longitudinal stability about its trim condition.

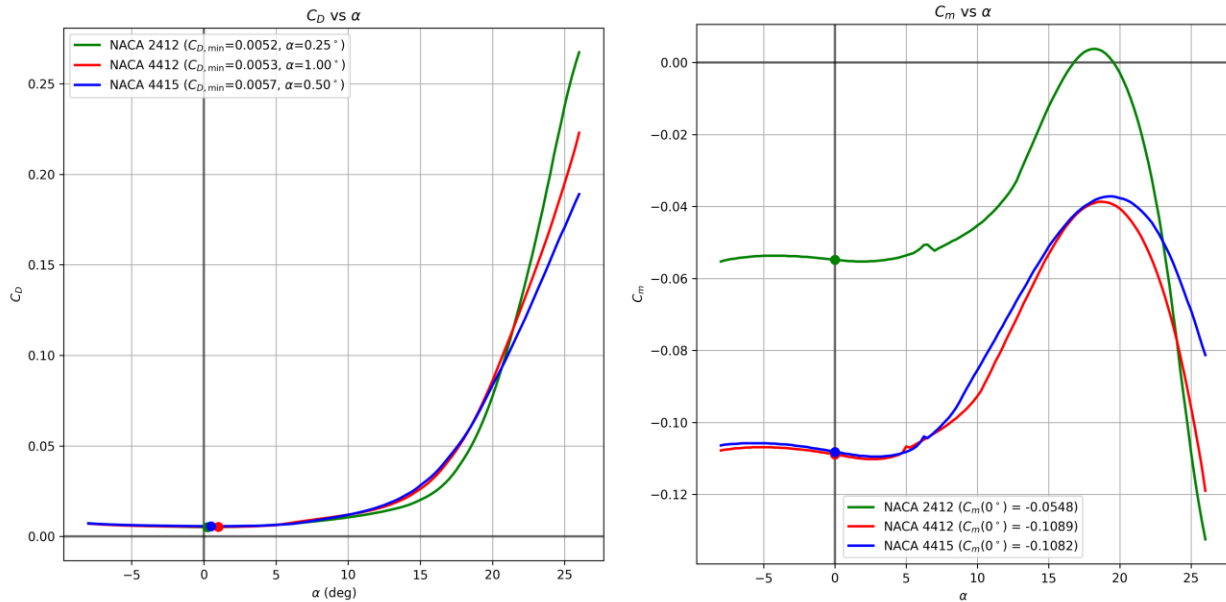


**Figure 3.3** Drag and pitching-moment coefficients versus angle of attack for the NACA airfoils.

The aerodynamic results presented in Figures 3.1 through 3.3 highlight consistent performance advantages of the NACA 44-series over the 2412, particularly in lift capability, efficiency, and stability. To quantify these findings and assess their overall suitability for the agricultural mission profile, a deterministic selection matrix was developed, incorporating aerodynamic, structural, and operational criteria.

### 3.2 Selection Matrix

To translate the aerodynamic results into a quantitative design decision, a deterministic selection matrix was developed to evaluate each airfoil based on four primary criteria: maximum lift coefficient ( $C_{L,\max}$ ), maximum lift-to-drag ratio ( $C_L/C_D$ )<sub>max</sub>, minimum drag coefficient ( $C_{D,\min}$ ), and relative thickness. These parameters capture the core aerodynamic and structural considerations that govern low-speed, high-lift agricultural aircraft performance.

**Table 3.3** Key Airfoil Aerodynamic Characteristics

Airfoil	$C_{L,\max}$	$C_L/C_D$ max	$C_{D,\min}$	Thickness (%)
NACA 2412	1.8887	137.4	0.0052	12
NACA 4412	1.958	172.19	0.0053	12
NACA 4415	1.9269	174.13	0.0057	15
Mean	1.9245	161.24	0.0054	13

As shown, the NACA 4412 and 4415 both outperform the 2412 in terms of lift and efficiency, while the 4415 provides additional structural depth from its thicker profile. Although the 4415 has a marginally higher minimum drag coefficient, this penalty is offset by its increased thickness ratio and comparable  $C_L/C_{D \text{ max}}$ .

To enable an equitable comparison across parameters of differing magnitudes, each metric was normalized by the mean or target value and assigned a weighting factor reflecting its relative importance to the agricultural mission. The weighting emphasizes aerodynamic performance ( $C_{L,\text{max}}$  and  $C_L/C_{D \text{ max}}$ , 0.35 each), while also accounting for structural and efficiency considerations ( $C_{D,\text{min}}$  0.15, thickness 0.15). The resulting normalized scores and overall performance indices are presented in Table 3.4.

**Table 3.4** Airfoil Selection Matrix

Airfoil	$C_{L,\text{max}}$	$C_L/C_{D \text{ max}}$	$C_{D,\text{min}}$	Thickness (%)	Score
Normalized Equation	X/1.9245	X/161.24	0.0054/X	X/13	
Weight	0.35	0.35	0.15	0.15	1
NACA 2412	0.3435	0.2983	0.1558	0.1385	0.9360
NACA 4412	0.3561	0.3738	0.1528	0.1385	1.0211
NACA 4415	0.3504	0.3780	0.1421	0.1731	1.0436

The NACA 4415 achieved the highest composite score (1.04), narrowly surpassing the 4412 (1.02) and significantly outperforming the 2412 (0.94). The results reinforce the trends observed in the aerodynamic plots: both 44-series airfoils deliver higher lift and efficiency, but the 4415's additional thickness offers practical structural benefits for heavy-load agricultural missions. Accordingly, the NACA 4415 was selected as the baseline main-wing airfoil for subsequent design and optimization. Its combination of high  $C_{L,\text{max}}$  and structural robustness makes it ideally suited for the operational profile of a modern agricultural aircraft.

### 3.3 Wing Sizing

According to *Aircraft Design: A Conceptual Approach*, agricultural aircraft typically exhibit an aspect ratio of approximately 7.5, as listed in Table 4.1 (Raymer, 2018). However, comparison with real-world aircraft models—summarized in Table 3.1—indicates that operational designs tend to employ slightly higher aspect ratios, averaging near 8.5. This value is representative of both lighter configurations, such as the Cessna 188, and heavier designs, such as the Air Tractor 802A. Because the current configuration is intended to represent a high-

Conceptual Design Report

capacity agricultural aircraft operating at the upper end of the mass range, the Air Tractor 802A serves as the reference for establishing the design aspect ratio.

Based on the derived aspect ratio for the Air Tractor AT-802 and an assumed wetted-area ratio of 4, estimated from Figure 3.6 in *Aircraft Design: A Conceptual Approach* (Raymer, 2018), the corresponding wetted aspect ratio is calculated as 2.185. Applying Equation 3.12 from the same reference and assuming a KLD value of 9—appropriate for non-retractable propeller aircraft—the maximum lift-to-drag ratio,  $(L/D)_{max}$ , is determined to be 13.3. This value serves as the aerodynamic efficiency parameter used throughout the subsequent performance analyses.

The next step in the geometric design process is the determination of the main wing size. Using the previously established true aspect ratio ( $AR=8.74$ ) and adopting a baseline wing loading of  $25 \text{ lb}/\text{ft}^2$  in conjunction with a gross weight estimate of 13,000 lb (discussed in Section 3.4), the primary wing area and span can be determined. The wing planform area,  $S_w$ , is estimated to be approximately  $520 \text{ ft}^2$ . The wingspan,  $b_w$ , is then calculated using the standard aspect ratio relationship:

$$AR = \frac{b^2}{S_w}$$

Substituting the known values yields a wingspan of 66.5 ft. Consequently, the mean aerodynamic chord,  $\bar{c}$ , is determined to be 7.8 ft.

To maintain consistent proportions with comparable agricultural aircraft, the fuselage length was estimated using the empirical relationship and coefficients provided in Table 6.3 of *Aircraft Design* (Raymer, 2018). For agricultural configurations, the coefficients  $a = 4.04$  and  $C = 0.23$  yield a fuselage length of approximately 36 ft, which aligns well with the proportions of the Air Tractor series and Thrush aircraft families.

Tail geometry was determined using the empirical tail volume coefficient method described in Equations 6.28 and 6.29 of *Aircraft Design* (Raymer, 2018). Typical volume coefficients for agricultural aircraft are  $C_{VH} = 0.5$  for the horizontal tail and  $C_{VT} = 0.04$  for the vertical tail. Assuming a tail-arm length of approximately 18 ft—roughly one-half of the fuselage length—measured between the quarter-chords of the main wing and horizontal tail, the horizontal tail area is estimated to be  $112.67 \text{ ft}^2$ , while the vertical tail area is approximately  $76.82 \text{ ft}^2$ .

These sizing results are consistent with the proportions observed in operational agricultural aircraft (Air Tractor AT-802, Thrush 710p), ensuring adequate longitudinal and directional stability for low-altitude operations, high-lift configurations, and slow-speed maneuvering.

## 4. Propulsion

### 4.1 Engine Selection

To select an engine for our crop duster, four constraints were taken into account to identify possible engine options. The first constraint considered for engine selection was the SFC (specific fuel consumption). To be able to crop dust 400 acres of land for the design mission and achieve a cruise range of 600 nm, an estimated engine SFC between 0.5 and 0.6 was needed.

The next constraint considered for engine selection was the weight of the engine. Based on historical data for crop duster engines, the weight of the engine needed to be about 3–5% of the aircraft's empty weight. Taking the high end of that range (5%), the engine for our aircraft needed to be under 650 lbs, or approximately 5% of 13,000 lbs.

The third constraint considered for engine selection was the takeoff distance requirement. Our crop duster was limited to a takeoff distance of 1,500 ft to clear a 50-ft obstacle. According to Raymer's Figure 5.4, this meant our aircraft needed to have a TOP value under 175. Using the TOP equation from Raymer's Figure 5.4, with an estimated W/S of around 25, a density ratio of about 0.95, an aircraft weight of approximately 13,000 lbs, and a lift-off coefficient of lift of about 1.3 our engine's horsepower needed to be over 1,500. With 1,500 hp, the aircraft was able to clear a 50-ft obstacle in 1,500 ft, meeting the design requirement.

The final restriction for our crop duster engine was that it had to be Agriculture Certified. For an aircraft to legally be used as a crop duster, its engine must be Agriculture Certified under FAA Part 33 (engine certification) and Part 137 (agricultural aircraft operations). An Ag-certified engine is one that has been built and tested to handle harsh environments where the engine ingests large amounts of dust, pollen, and chemicals while operating at low altitudes and air speeds on hot days. It also must be capable of withstanding constant throttle changes and unpaved takeoff and landing strips near fields.

**Table 4.1** Engine Requirements

Engine Requirements	Power (hp)	Weight (lbs.)	SFC	Ag Certified
	Over 1500	Under 650	Under 0.6	Yes

Using the requirements above, a list of engines that met all criteria was created. Due to the size of the crop duster we are designing, a high-horsepower engine is required. Engines with at least 1,500 hp that are Ag-certified are rare, meaning we only found two options that met the necessary requirements. The two engines were the PT6A-67F by Pratt & Whitney and the TPE331-14AG by Honeywell Aerospace. Due to the small selection of engines that we could choose from we also investigated smaller engines in case we ever decide to downsize our aircraft. The PT6A-67AG Pratt & Whitney is the engine that most closely meets the necessary

Conceptual Design Report

requirements but was disregarded due to the low horsepower of 1,350. Data for the PT6A engines was obtained from the European Union Aviation Safety Agency's study on the PT6A-67 aircraft series and *Jane's Aero Engines*. Data for the TPE331-14AG was obtained from Honeywell Aerospace TPE331-14 data sheet and *Jane's Aero Engines*. For now, the two engines that met the requirements were put into a selection matrix to decide between them.

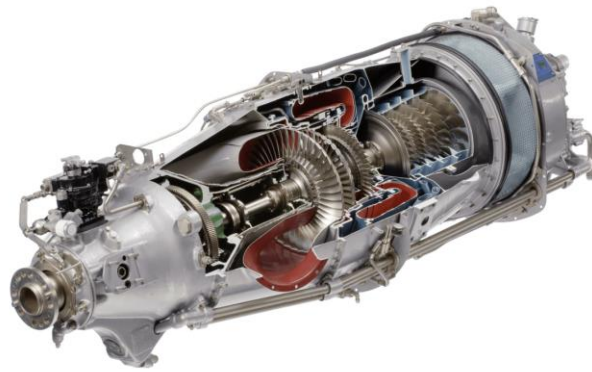


**Figure 4.1: PT6A Engine**



**Figure 4.2: TPE331 Engine**

For the selection matrix, four variables were considered: engine power, engine weight, SFC of the engine, and engine volume. When weighing the importance of each category, power was by far the most important. We want our crop duster to be able to carry as large a payload as possible while meeting the takeoff requirements, so we gave it a weight of 0.5. Weight and SFC were listed as the next most important variables when selecting an engine, as both affect the aircraft's range. Additionally, lower weight allows for easier takeoff conditions. Engine volume was listed as the least important factor since the airframe can be designed around it, although a smaller size is still preferable.

With the weights decided, the normalized requirement equations for each variable were created. For power, the equation was  $X / 1675$ , because 1,675 hp is the average power between

## Conceptual Design Report

the engines, and it is in the denominator since more power is better. For weight, the equation was  $596 / X$ , because 596 lbs. is the average weight between the two engines, and it is in the numerator since a lower weight is better. For SFC, the equation was  $0.55 / X$ , because an SFC value between 0.5 and 0.6 is desired, and a lower SFC is better. Finally, for volume, the equation was  $15.5 / X$  was used because  $15.5 \text{ ft}^3$  was the average volume between the two engines, and a lower volume is better.

**Table 4.2 Selection Matrix**

Engine	Power (hp)	Weight (lbs)	SFC (lb/hp/hr)	Volume (ft <sup>3</sup> )	Sum
Normalized Requirement	X/1675	596/X	0.55/X	15.5/X	
Weight	0.5	0.2	0.2	0.1	1
PT6A-67F	0.50746268	0.208391608	0.192982456	0.134782609	1.04361936
TPE331-14AG	0.49253731	0.192258065	0.215686275	0.077114428	0.97759608

**Table 4.3 Engine Specifications**

Engine	Power (hp)	Weight (lbs)	SFC	Volume (ft <sup>3</sup> )
PT6A-67F	1700	572	0.57	11.5
TPE331-14AG	1650	620	0.51	20.1

After performing the selection matrix, the PT6A-67F had the highest score of 1.04 while the TPE331-14AG had a score of 0.98. Overall, by looking at the specifications of the engines the PT6A-67F was superior in almost every category and is the obvious choice for our engine.

## 4.2 Propeller Diameter

To estimate the diameter of our aircraft's propeller, equations (10.21), (10.22), and (10.23) from *Raymer (2018)* were used. By combining Equations (10.21) and (10.22), the following expression can be obtained to calculate the maximum allowable propeller diameter:

$$D_{max} = \frac{\sqrt{V_{limit}^2 - V_{forward}^2}}{\pi n}$$

In this equation,  $V_{limit}$  is the maximum allowable tip speed for the propeller,  $V_{forward}$  is the maximum flight speed, and  $n$  is the rotational rate of the engine. Since our aircraft was designed to be more rugged, we used metal propellers, which according to Raymer have a maximum tip speed of 950 ft/s. To match the Air Tractor At-802's performance, we also assumed a maximum flight speed of 190 knots. This speed keeps the aircraft below the FAA's 250 knot limit for

operations under 10,000ft. Using data from the PT6A-67F engine,  $n$  was taken as 1,700 rpm.

Converting everything into constant units gave us an initial estimate of 120 inches.

Using equation (10.23), another estimate for the propeller diameter was obtained:

$$D_{max} = K_p \sqrt[4]{Power}$$

According to Raymer, an aircraft with four or more blades has a  $K_p$  value of 1.5. Using that  $K_p$  value and the power value of 1,700 hp from our engine, we were able to get a second estimate of 115 inches. As Raymer recommended, the smaller of the two estimated values was selected, meaning our initial propeller diameter for our design was calculated to be 115 inches.

## 5. Structural Analysis

### 5.1 FEA

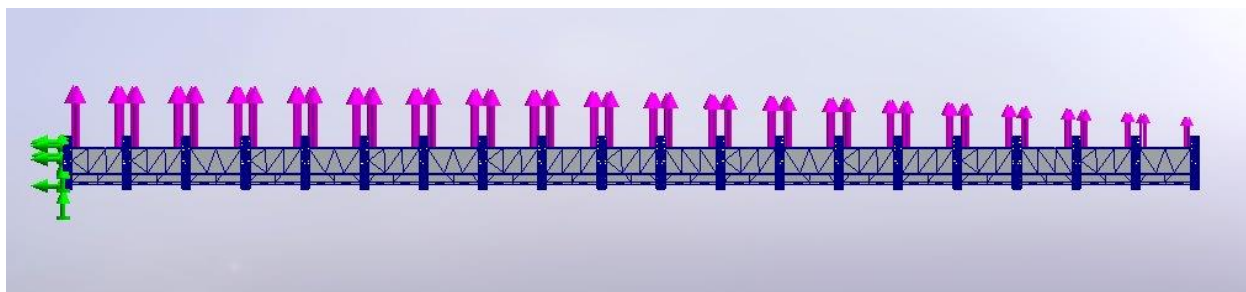


**Figure 5.1** Elliptical lift distribution on wing

The finite element analysis (FEA) was conducted on a half-wing model to assess the structural performance under aerodynamic loading representative of maximum takeoff conditions. The applied load was set to 6,300 lb—half of the aircraft’s max takeoff weight (MTOW)—distributed elliptically along the quarter-chord line to replicate realistic lift behavior. The main spar, constructed as an I-beam, carried the majority of bending loads while minimizing torsional effects due to its placement at the quarter chord. This configuration accurately captured the distribution of lift forces and bending moments across the span, avoiding the root overestimation common with uniform loading assumptions.

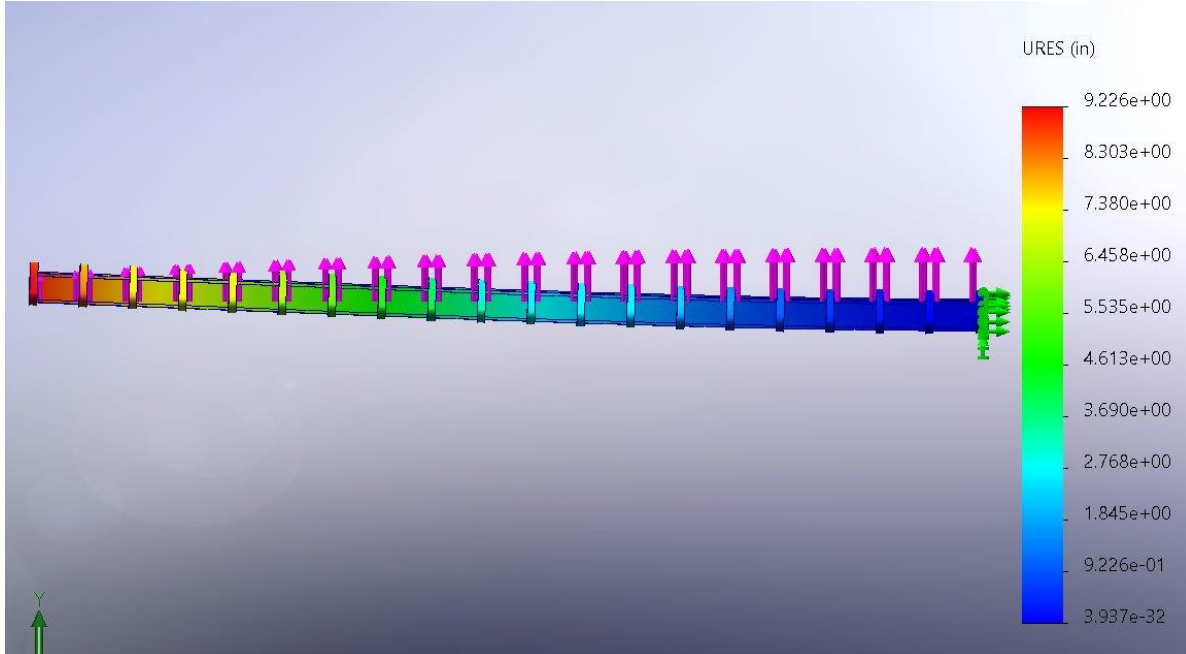


**Figure 5.2** Wing flexure in inches under MTOW load

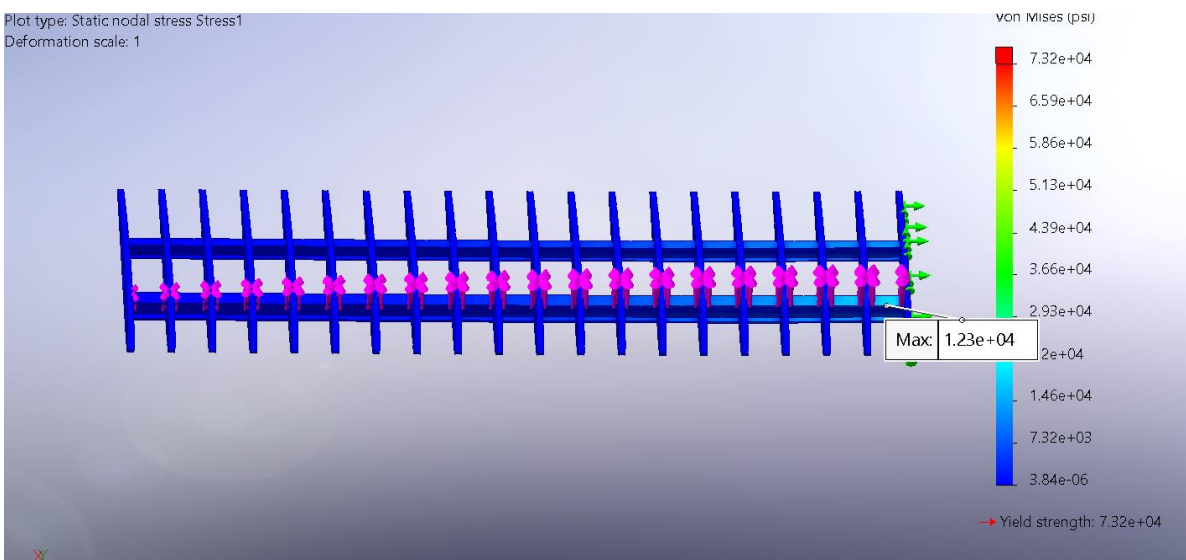


**Figure 5.3** Stress analysis on half-wing with MTOW load

The material chosen for the analysis was aluminum 7075-T6 due to its prevalent use in the general aviation industry. The stress field seen in fig. 5.3 showed a maximum von Mises stress of roughly  $1.23 \times 10^4$  psi, well below the  $7.3 \times 10^4$  psi yield strength of aluminum 7075-T6, confirming ample strength margin. Local stress concentrations were limited to spar attachments, and the analysis enabled the removal of non-critical material to reduce overall wing weight. Under limit aerodynamic loading, the wing exhibited a tip deflection of approximately 9 inches as seen in fig 5.2, corresponding to about 2.5 % of the half-span. This deflection falls

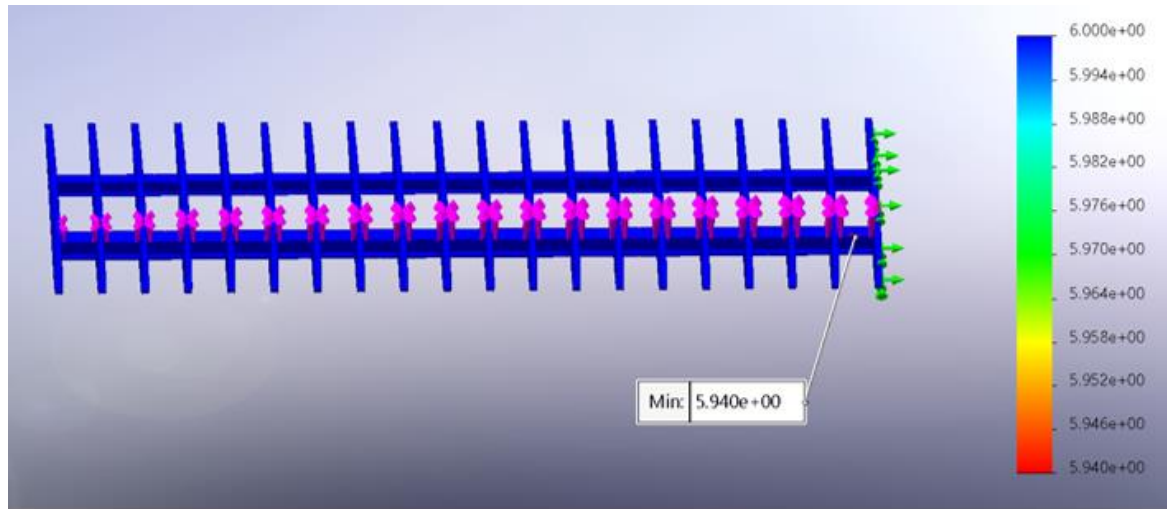


**Figure 5.4** Factor of safety analysis under MTOW load

The computed factor of safety averaged about 6 at maximum takeoff weight, with a minimum local FOS of 5.94. This reserve capacity not only provides robustness during agricultural maneuvering but also ensures wing-box integrity after payload release, when dynamic load changes occur. Overall, the FEA results verify that the wing structure achieves a conservative yet efficient balance between strength, stiffness, and weight for the operational envelope of the crop-duster.

## 5.2 V-n Diagram

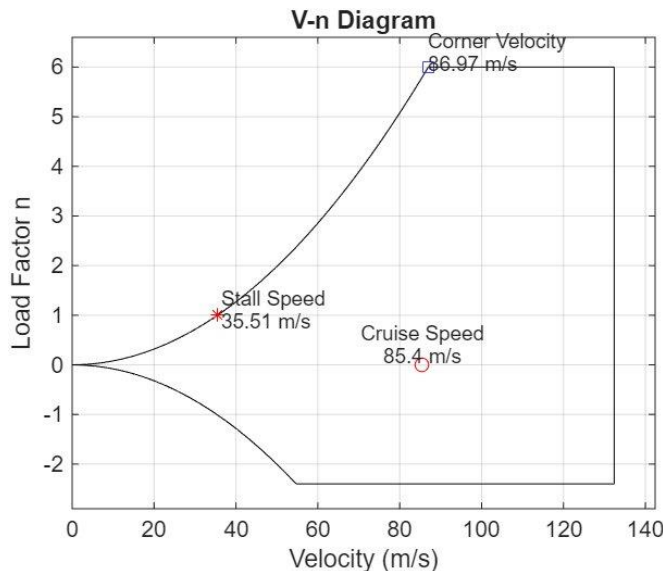


**Figure 5.5** V-n Diagram for crop duster

Figure 5.5 presents the V–n diagram for the crop duster, showing the aircraft’s operational envelope in terms of velocity and load factor. The stall speed is approximately 35.5 m/s (69 kt), representing the lower boundary of flight. The corner velocity, about 86.9 m/s (169 kt), marks the intersection of the maximum lift capability and the structural load limit—here roughly  $n = 6$ , indicating the highest load factor that can be sustained before structural limits are reached. This corresponds with the results from the FEA. The cruise speed of 85.4 m/s (166 kt) lies just below this corner point, demonstrating that the design maintains a wide and efficient operating margin between stall and maneuver boundaries.

The diagram reflects a robust airframe capable of sustaining large maneuvering loads, which is essential for agricultural operations involving steep pull-ups and low-altitude turns. The positive side of the envelope extends to about +6 g, while the negative side reaches roughly –2 g, consistent with reinforced agricultural-category aircraft under FAA Part 23 and 137 criteria. This wide envelope ensures that the aircraft can safely handle abrupt maneuvers and gust encounters during low-level spraying without exceeding structural limits. Overall, the V–n diagram confirms that the wing and control system design provide sufficient strength, maneuverability, and safety margin for demanding crop-dusting missions.

With no margin for error, the max load per wing is calculated as,

$$\text{Max Load on Wing} = \frac{\text{MTOW} \cdot n_{max}}{2} = \frac{12,600 \cdot 6}{2} = 37,800 \frac{\text{lbf}}{\text{wing}}$$

(5.2)

However, dividing by 1.5 as to provide a safety buffer before approaching the yield limit of the aluminum yields,

$$\text{Max Load on Wing} = \frac{\text{MTOW} \cdot n_{max}}{1.5 \cdot 2} = \frac{12,600 \cdot 6}{1.5 \cdot 2} = 25,200 \frac{\text{lbf}}{\text{wing}}$$

(5.3)

Similarly, we can calculate that the maximum load factor per wing at MTOW, with a safety buffer, is

$$\text{Max Load Factor per Wing at MTOW} = \frac{n_{max}}{1.5} = \frac{6}{1.5} = 4$$

(5.4)

Which provides ample room for maneuvering when fully loaded.

### 5.3 Dihedral

A moderate dihedral angle was selected to enhance the aircraft's lateral stability during low-altitude operations while maintaining responsive roll control. Crop dusters operate close to the ground and often fly in turbulent air, where gusts and crosswinds can quickly disturb the roll attitude. The dihedral provides a restoring rolling moment when the aircraft is displaced by sideslip—helping it naturally return to level flight without excessive pilot input. A modest geometric dihedral of about  $3^\circ$  was sufficient to achieve the desired stability without introducing sluggish roll response.

### 5.4 Sizing

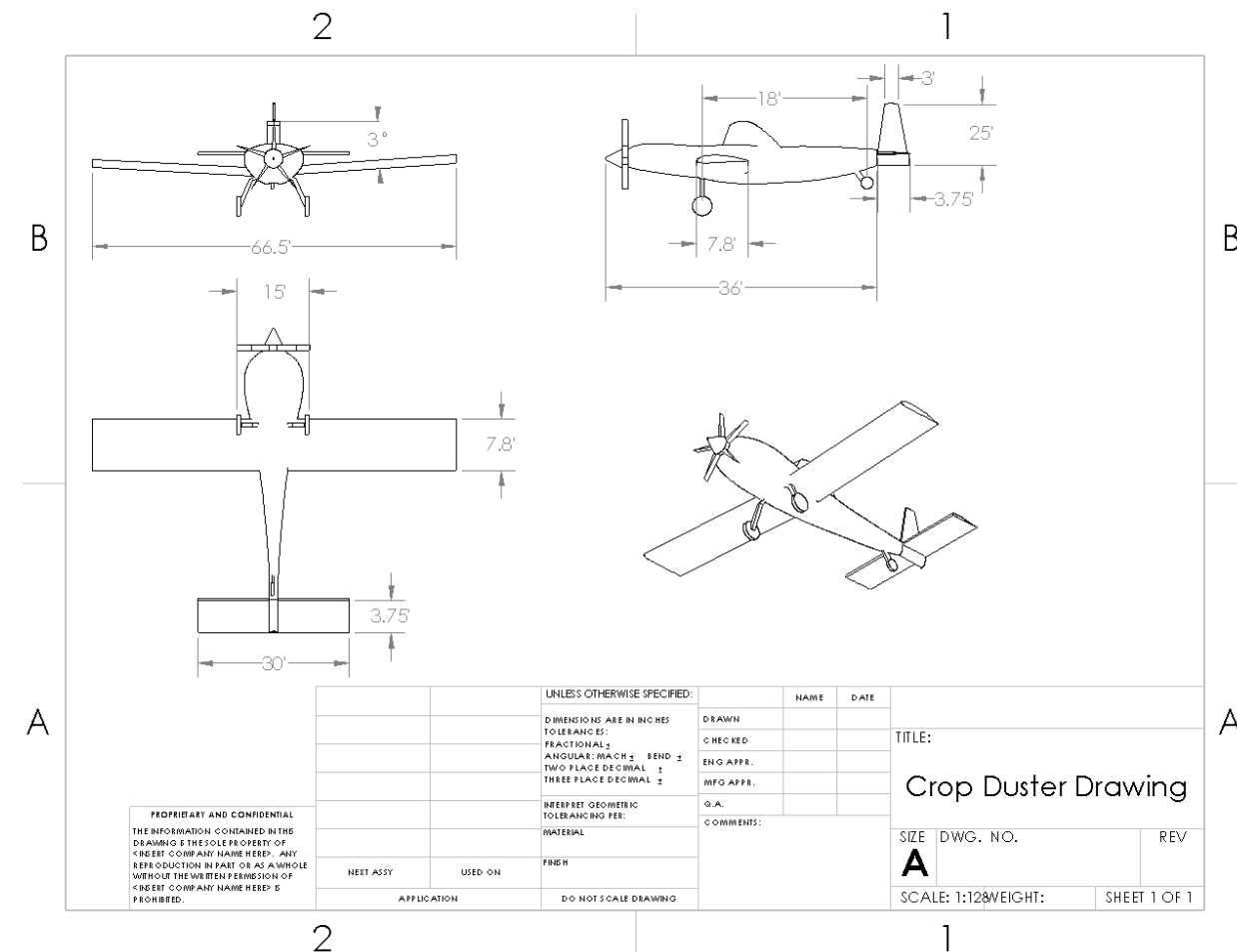


**Figure 5.6** Aircraft sizing sketch

## 6. Cost Analysis

### 6.1 Weight Based Analysis

For our initial cost analysis Rayner compares aircraft to bologna in the way that aircraft are similarly bought by the pound. However, for this procedure of cost analysis he provides a range of cost per pound in 1988 dollars. Which not only is massively outdated with inflation rates, but it also is quite a large range being 150-300 dollars per pound. So, in order to make this method any what accurate for our application I have decided to reference the Air Tractor AT-802 to find a cost per pound that not only is adjusted for inflation but is specific for our application.

The first step was to find the cost of a 2025 model of the Air Tractor 802A, which proved harder than imagined since Air Tractor doesn't post their prices on any official website. However, I happened to find an Iowa Department of Transportation list for registration cost of aircraft that had the list price of the 2025 model listed as \$2,370,000. This lines up with resale values of older models. Raymer estimates Defense Contractors Planning Report (DCPR) as 60-70 percent of the empty weight. The empty weight of the Air Tractor 802A is approximately 6,500lbs. This gives our cost per pound of a 2025 agricultural plane being around \$560.9.

Using our estimates for our we find the empty weight fraction of the design mission to be 0.5539, and for the ferry mission a value of 0.5729. To get a high ensd estimate I'll use the fraction for the ferry mission. Next for our gross weight we have estimated 13,000lbs for the design mission. For our estimate we use the empty weight to be around 7,200lbs. In turn this gives our DCPR weight to be 4,680lbs. Therefore, the estimated cost of the aircraft is \$2,625,012.

However, this is an extremely rough estimate used only for a first step heuristic and not a standalone method. So, as we sure up more of our design I will be able to use the RAND DAPCA-IV model to improve our estimate.

### 6.2 DAPCA-IV Model

For our more in-depth cost analysis, we used the RAND DAPCA-IV model mentioned in class. The DAPCA-IV model is a cost estimating software developed in 1986, in order to help estimate the development and production costs of military aircraft. This helps with our cost analysis, however, there are glaring issues in it we must address. Being developed 30 years ago makes the base model and constants extremely out of date due to inflation. There is also the issue of all of the labor rates I could find from 2012. So, to account for inflation I used the consumer price index (CPI) for 1998, 2012, and 2025 to find an accurate inflation trend. Using 163.0, 229.6, and 310.0 respectively as our CPI's we found the inflation factor from 1998 to 2012 to be 1.408. Similarly, the inflation factor from 2012 to 2025 was found to be 1.350.

For the model itself it is based on a set of equations that are used to find costs related to research, development, testing, and evaluation. The first of these being engineering manhours,

$$H_e = 4.86 * W^{.777} * V^{.894}_{max} * Q^{.163}$$

Conceptual Design Report

Where W is empty weight, V is maximum velocity, and Q is the production quantity. The other equations used in the DAPCA-IV model for our cost estimation are listed below, all of which are in FPS units.

Where T is tooling manhours:

$$T = 5.99 * W^{.777} * V^{.696}_{max} * Q^{.641}$$

Where L is manufacturing labor manhours:

$$L = 7.37 * W^{.82} * V^{.484}_{max} * Q^{.641}$$

Where QC is quality control manhours:

$$QC = .13 * L$$

Where D is development support cost

$$D = 66 * W^{.63} * V^{1.3}_{max}$$

Where F<sub>test</sub> is flight test cost and Q<sub>D</sub> is the number of aircraft for flight testing and development:

$$F_{test} = 1852 * W^{.325} * V^{.822}_{max} * Q_D^{1.21}$$

Where M is manufacturing materials cost:

$$M = 16.39 * W^{.921} * V^{.621}_{max} * Q^{.799}$$

For the engine cost we decided to use the following equation using the values of the PT6A-67F:

$$P = 2306[0.043 * T_{SLS} + 243.3 * M_{max} + .969 * T_R - 2228]$$

Where P is the production cost in 1998 dollars, which will be adjusted for inflation, where T<sub>SLS</sub> is sea level maximum thrust, M<sub>max</sub> is the maximum Mach number, and T<sub>R</sub> is the turbine inlet temperature in Rankin. For the avionics we can approximate it as \$4,000 to \$8,000 per pound of aircraft in 2012 dollars. Since our avionics is likely to be on the expensive side, we used \$8,000 and then accounted for inflation.

Putting all of this together this gives our total program cost to be 738 million dollars, which comes out to around 9.228 million per aircraft. This is assuming our initial production quantity is 80 aircraft, however, if we change our planned production quantity to something like 300, we see the total program cost increases to 1101.52 million, but the cost per aircraft drops significantly to only 2.57 million per aircraft which is exactly in line with what we would expect. This shows a larger initial investment is required to make the program profitable. A breakdown of the RDT&E and production costs is shown in figure 6.1 for a production quantity of 300.

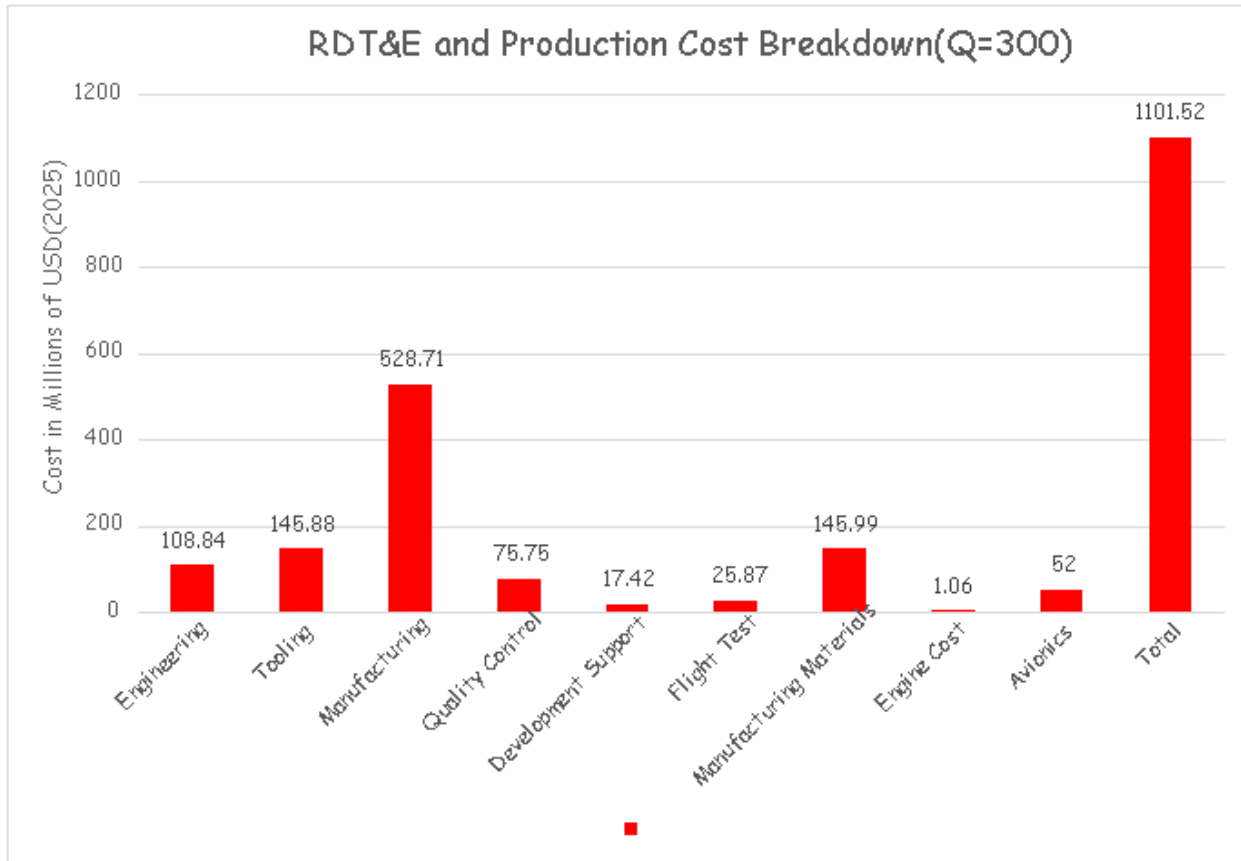


**Figure 6.1 RDT&E and Production Cost Breakdown**

From this we can isolate the production costs of the airplane and calculate flyaway cost per aircraft. It comes out to be approximately 3.2 million dollars per aircraft, which is expensive but within what we could expect from our analysis thus far.

Next, we move onto the breakeven analysis where we used a 20% profit margin to calculate revenue versus cumulative cost.

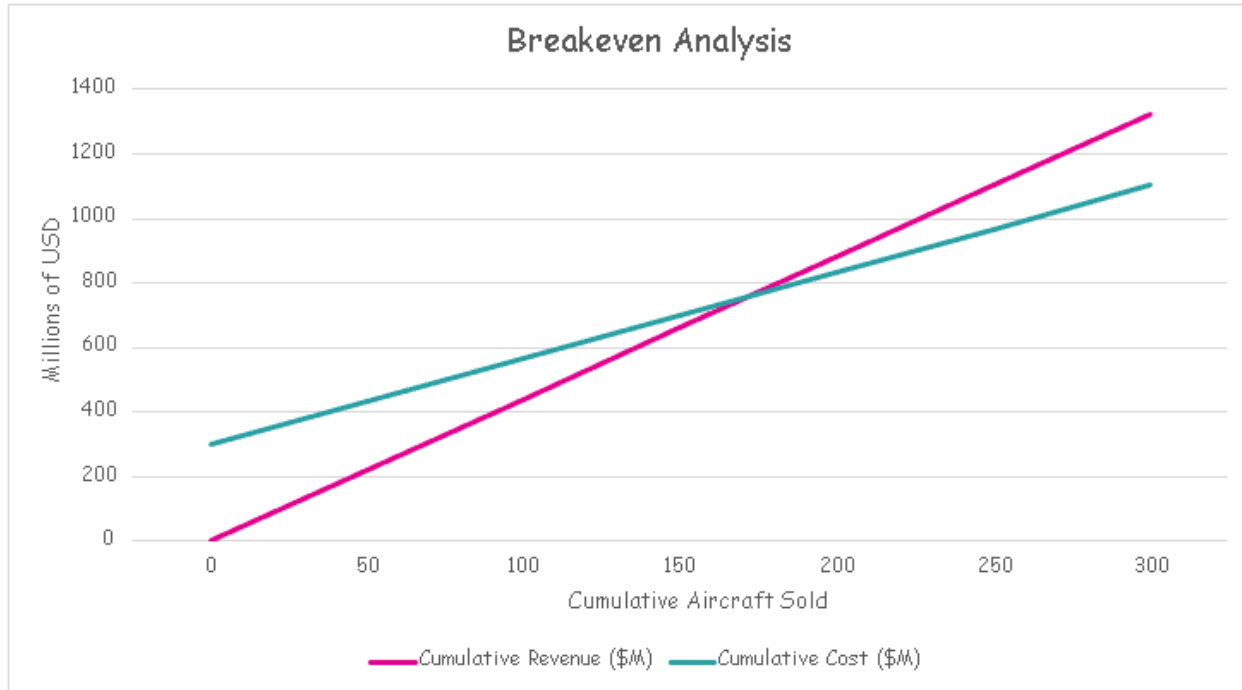


**Figure 6.2** Breakeven Analysis

From this we can see that the breakeven point would be around 180 aircraft manufactured. We could possibly lower this by advertising our autopilot crop duster as a premium aircraft and potentially up the profit margin, which in turn would allow us to breakeven with this project sooner if needed.

## 7. Conclusion

This conceptual design represents the first phase in developing an efficient and reliable agricultural aircraft capable of meeting modern performance and safety standards. Using established methods from Raymer's *Aircraft Design: A Conceptual Approach* and direct comparison with existing crop-dusting aircraft, a feasible baseline configuration was developed. The selected NACA 4415 airfoil, PT6A-67F turboprop engine, and 66.5 ft wingspan collectively provide a balanced combination of lift capability, stability, and propulsion performance suited to low-altitude agricultural operations. Finite element and performance analyses demonstrate that the proposed configuration achieves the required structural strength, stiffness, and maneuvering capability. The estimated cost further aligns with comparable aircraft, indicating consistency with real-world production trends. As an initial study, this report presents a viable foundation for a modern agricultural aircraft design capable of achieving its intended operational objectives.

## References

- Dataintelo, Sharma, R., & Dataintelo. (2024, December 3). *Agricultural Aircrafts Market Report | Global Forecast from 2025 to 2033*. Dataintelo.  
<https://dataintelo.com/report/agricultural-aircrafts-market#:~:text=The%20global%20agricultural%20aircrafts%20market,expected%20to%20experience%20significant%20growth>
- European Union Aviation Safety Agency (EASA). (2022, February 18). *Type certificate data sheet: PT6A-67 series engines (Issue 06, No. EASA.IM.E.008)*. Pratt & Whitney Canada Corp.  
<https://www.easa.europa.eu/en/document-library/type-certificates/im-e-008>
- Gunston, B. (Ed.). (2018). *Jane's Aero Engines 2018–2019*. Coulsdon, Surrey, United Kingdom: IHS Markit.
- Honeywell Aerospace. (n.d.). *TPE331-14 turboprop engine*. Scribd.  
<https://www.scribd.com/document/331799918/TPE331-14-Turboprop-Engine>
- Kalake, A. (2024, August 14). *Agricultural Aircrafts Market Size, scope, Growth and Forecast*. Verified Market Research.  
<https://www.verifiedmarketresearch.com/product/agricultural-aircrafts-market/>
- Luxhøj, J. T. (2015). *A Socio-technical Model for Analyzing Safety Risk of Unmanned Aircraft Systems (UAS): an application to precision agriculture*. *Procedia Manufacturing*, 3, 928–935.  
<https://doi.org/10.1016/j.promfg.2015.07.140>
- Raymer, D. P. (2018). *Aircraft Design: A Conceptual Approach* (6th ed.). American Institute of Aeronautics and Astronautics (AIAA).
- Sivakumar Ramakrishnan (2025). *V-n Diagram*.  
<https://www.mathworks.com/matlabcentral/fileexchange/81793-v-n-diagram>, MATLAB Central File Exchange. Retrieved October 5, 2025.
- Uddin, M. N. (2025, September 23). *Aircraft manufacturers market share: Global leaders unveiled - MACROTER*. NasEcom. <https://macroter.com/aircraft-manufacturers-market-share/>
- Van Doorn, R. R. A. (2014). *Accidents in agricultural aviation in the United States*. *Aviation Psychology and Applied Human Factors*, 4(1), 33–39. <https://doi.org/10.1027/2192-0923/a000053>